Hindawi
International Transactions on Electrical Energy Systems
Volume 2023, Article ID 6678942, 14 pages
https://doi.org/10.1155/2023/6678942

Research Article

A Data-Driven Approach for Reactive Power Optimization Incorporating Interval Values for Renewable Power Generation

Honglei Jia,[1] **Cong Zhang**,[1] **Jieming Du**,[1] **and Na Kuang**[2]

[1]*College of Electrical and Information Engineering, Hunan University, Changsha, China*
[2]*School of Educational Science, Hunan Normal University, Changsha, China*

Correspondence should be addressed to Cong Zhang; zcong@hnu.edu.cn

Received 2 December 2022; Revised 12 September 2023; Accepted 28 September 2023; Published 21 October 2023

Academic Editor: Salvatore Favuzza

The increasing integration of renewable energy sources into modern electric grids has led to a rise in uncertain factors that must be managed to maintain voltage security during reactive power optimization (RPO). Traditional deterministic RPO methods fail to account for these uncertainties, which can result in power grid security issues such as voltage violations. To address these challenges, this paper proposes a data-driven interval-based reactive power optimization method (IRPOM). The IRPOM represents the uncertainties associated with renewable power generation and load demands as intervals within the RPO problem formulation. The proposed method uses an improved particle swarm optimization algorithm to solve the RPO problem. In each iteration, the uncertain power flow is solved using the optimizing-scenarios method- (OSM-) based interval power flow (IPF) algorithm. This approach calculates the real power losses and checks whether state quantities, including voltage, power flow, and generator output, exceed their limits. Furthermore, a data-driven modeling approach is introduced to reduce the conservativeness of the IRPOM solutions. The effectiveness of the proposed method is demonstrated through detailed computational analysis on a modified IEEE 30-bus system. The results show that the proposed approach ensures economic efficiency while maintaining a low bus voltage threshold crossing probability close to zero.

1. Introduction

The increasing integration of large-scale renewable power generation into electric power networks has a significant impact on their operational security, owing to the inherent uncertainties in renewable power outputs [1–3]. The reactive power optimization (RPO) is crucial for the safe integration of large-scale renewable energy generation into the power grid. The primary goal of RPO is to optimize the placement of reactive compensators and transformer tap ratios, ensuring voltage stability and minimizing real power losses while considering the inherent variability and intermittency of renewable power sources. This proactive approach is essential for maintaining grid reliability, improving operational safety, and achieving seamless integration of renewable energy sources into the power grid.

Despite extensive research and application in both academia and industry, reactive power optimization (RPO) under high levels of renewable energy source integration into the power grid faces significant challenges [4, 5]. Dealing with various large-scale uncertain data in the RPO process poses formidable challenges for decision-makers. Ensuring robust and accurate decision-making processes becomes crucial, as underestimating or overestimating the impact of uncertainties can severely jeopardize the stability and reliability of the power grid. Consequently, traditional deterministic RPO methods are inadequate in guaranteeing the safe and stable operation of the power system.

In recent years, several optimization methods have been developed to address the uncertainties arising from the high levels of renewable energy integration and ensure the reliability of reactive power optimization (RPO) decisions [6, 7], such as the probabilistic approach method (PAM) [8, 9], the scenario analysis method (SAM) [10, 11], the robust optimization method (ROM) [12, 13], and the interval optimization methods (IOM). The main

difference among these methods lies in their approaches in describing the uncertainty of input parameters.

PAM utilizes probability density functions (PDF) to describe the uncertainty of input parameters, with a strong reliance on historical data. For example, in the case of solar irradiance, the PDF is obtained through non-Gaussian fitting and kernel density estimation. The generated PDF is then used in conjunction with backward/forward scan methods to address each scenario generated by the Monte Carlo simulation (MCS) method [14]. However, the MCS method is known for its time-consuming nature. To overcome this challenge in power systems with high levels of renewable energy integration, a stochastic optimal RPO method has been developed. This method uses cumulative quantities to generate PDF as linear combinations of uncertain variables. By doing so, complex convolution operations are avoided, leading to a reduction in computational time [15]. Similarly, a PAM method called probabilistic load flow (PLF) has been proposed, which utilizes Gaussian quadrature and takes into account voltage variations under uncertain loads [16]. However, in practical engineering problems, modeling uncertain parameters using PDF is often challenging due to economic and technical considerations [17, 18]. The SAM (scenario analysis method) tackles this issue by converting the continuous space of uncertain environments into a discrete finite set of scenarios with assigned probabilities [19]. For example, in long-term RPO, a multistage stochastic nonlinear model was introduced, where the uncertainty of loads demand was handled during the planning stage using efficient methods for scenario tree generation and scenario tree reduction [20]. However, one drawback of the SAM is that the computational time increases significantly as the number of scenarios to be considered grows, making it impractical for application in large-scale power systems. In contrast to the use of historical data in PAM, RO represents uncertain input parameters using parameter bounds [6]. For example, the uncertainty associated with wind turbine output and system loads is captured by defining a bounded interval within a polyhedral uncertainty set. This ensures that the optimal power flow remains unaffected by prediction errors in these two parameters [21]. Likewise, a two-stage linear ROM-based method has been developed to evaluate the range of reactive power and ensure the operational safety of wind farms in the presence of uncertain factors [22]. However, the design of ROM is not suited for nonconvex problems [23]. IOM takes a different approach by assuming that known intervals can be used to represent uncertain parameters. These intervals are then used to define the range of output variables without the need for explicit distribution functions, highlighting the significant engineering application value of IOM [24, 25]. Furthermore, IOM demonstrates effectiveness in addressing nonconvex problems. However, one drawback of the solutions provided by IOM is that they naturally include the worst-case scenarios within the uncertainty set. While this guarantees optimal results, it can also lead to overly conservative solutions [26].

This paper addresses the aforementioned challenges by proposing a data-driven interval reactive power optimization method (IRPM). The main work of this paper is summarized as follows:

(i) IRPM utilizes the interval optimization method (IOM) to handle uncertain variables, specifically addressing the voltage security issue caused by the uncertainty of power generation and load in the power grid.

(ii) To solve the uncertain power flow (UPF) and obtain real power losses, IRPM employs the optimizing-scenarios method (OSM)-based interval power flow (IPF) algorithm, significantly reducing computational complexity [27].

(iii) To reduce conservatism in the IPF algorithm based on OSM, a data-driven approach is adopted. Historical data and prior knowledge are utilized to correct the output range of wind turbines. Moreover, this approach ensures that the models developed for uncertain input variables are not limited to fixed-type and fixed-parameter models.

(iv) To handle discrete variables in reactive power optimization (RPO) that are not easily optimized, an improved particle swarm optimization (PSO) algorithm is applied. This addresses the premature convergence issue of the standard PSO algorithm and enhances convergence speed and accuracy through the implementation of various improvement strategies.

(v) The effectiveness of the proposed IRPM is demonstrated and thoroughly analyzed using computational results obtained from the modified IEEE 30-bus system. The results illustrate that IRPM is capable of finding optimal generator voltages, reactive power device inputs, and transformer tap ratios in the test system.

The organization of the remainder of this paper is as follows. Section 2 presents a detailed establishment of the model of RPO incorporation interval uncertainties (MRPOIU). Section 3 introduces the methodology applied to solve IRPM. Section 4 starts by introducing the parameters of the modified IEEE 30-bus system and then presents the simulation results and comparative verification results. Finally, Section 5 concludes the paper.

2. Establishment of the MRPOIU

The MRPOIU applies an objective function based on the combined cost of reactive power compensation devices, including the sum of the average annual investment costs and the annual costs of energy losses. Therefore, the model is expressed as follows:

$$\min f = \left[E\left(P_{\text{Loss}}\right) \cdot \rho_1 + \frac{C_\delta}{T_\delta} \cdot \rho_2 \right], \tag{1}$$

where $E(P_{\text{Loss}})$ is the annual energy losses, C_δ is the total reactive power compensation capacity, T_δ is the service life of reactive power compensation devices, ρ_1 is power grid price in ¥/KWh, and ρ_2 is the unit capacity investment cost in ¥/KVar.

The objective function is subject to the following constraints:

$$\begin{cases} -P_i = \left[\underline{P_{\text{L}i}}, \overline{P_{\text{L}i}}\right], \\ Q_{\text{C}i} - Q_i = \left[\underline{Q_{\text{L}i}}, \overline{Q_{\text{L}i}}\right], \\ P_{\text{L}i} + P_i = \left[\underline{P_{\text{G}i}}, \overline{P_{\text{G}i}}\right], \end{cases} \tag{2}$$

$$\begin{cases} Q_{\text{G}i,\min} \le Q_{\text{G}i} \le Q_{\text{G}i,\max}, \\ Q_{\text{l}i,\min} \le Q_{\text{l}i} \le Q_{\text{l}i,\max}, \\ Q_{ci,\min} \le Q_{ci} \le Q_{ci,\max}, \\ T_{l,\min} \le T_l \le T_{l,\max}, \\ V_{i,\min} \le V_i \le V_{i,\max}, \end{cases} \tag{3}$$

where formula (2) represents the active power and reactive power balance equations at the load bus and the balance equation at the generator bus and formula (3) represents the output limitations of reactive power generation, the capacity limits of the static VAR compensators (capacitive and inductive), the constraints on the tap positions of transformers, and the acceptable operating ranges of the voltage magnitudes (except for the slack bus). P_i is the nodal active power, Q_i is the nodal reactive power, $Q_{\text{C}i}$ is the reactive compensation at bus i, $P_{\text{L}i}$ is the active load demand at bus i, $Q_{\text{L}i}$ is the reactive load demand at bus i, the intervals $[P_{\text{G}i}, \overline{P_{\text{G}i}}]$, $[P_{\text{L}i}, \overline{P_{\text{L}i}}]$, and $[Q_{\text{L}i}, \overline{Q_{\text{L}i}}]$ are associated with active power generation, active power load demand, and reactive power load demand, respectively. $Q_{\text{G}i}$ is the reactive power generation of generator bus i, $Q_{\text{l}i}$ and Q_{ci} are the compensation capacity of the reactor and capacitor at bus i, respectively, T_l is the tap positions of transformers at branch l, V_i is the voltage magnitudes of bus i. $Q_{\text{G}i,\min}$ and $Q_{\text{G}i,\max}$ are lower and upper bounds of the reactive power generation of generator bus i, respectively, $Q_{\text{l}i,\min}$ and $Q_{\text{l}i,\max}$ are lower and upper bounds of the compensation capacity of the reactor at bus i, respectively, $Q_{ci,\min}$ and $Q_{ci,\max}$ are lower and upper bounds of the compensation capacity of the capacitor at bus i, respectively, $T_{l,\min}$ and $T_{l,\max}$ are lower and upper bounds of the tap positions of transformers at branch l, respectively, and $V_{i,\min}$ and $V_{i,\max}$ are lower and upper bounds of the voltage magnitudes of system bus i, respectively. In addition, the following equality conditions are applied:

$$\begin{cases} C_\delta = \sum_{i=1}^{\text{n}} (Q_{\text{l}i} + Q_{ci}), \\ E(P_{\text{Loss}}) = \dfrac{\overline{p_{\text{loss}}} + \underline{p_{\text{loss}}}}{2} \cdot 8760, \\ \begin{cases} Q_{\text{l}i} = \left|Q_{\text{C}i}\right|, Q_{ci} = 0\, Q_{\text{C}i} \le 0, \\ Q_{\text{c}i} = Q_{\text{C}i}, Q_{\text{l}i} = 0\, Q_{\text{C}i} \ge 0, \end{cases} \\ \begin{cases} P_i = V_i \sum_{j \in S} V_j \left(G_{ij} \cos\theta_{ij} + B_{ij} \sin\theta_{ij}\right), \\ Q_i = V_j \sum_{j \in S} V_j \left(G_{ij} \sin\theta_{ij} - B_{ij} \cos\theta_{ij}\right), \end{cases} \end{cases} \tag{4}$$

where $\theta_{ij} = \theta_i - \theta_j$, θ_i and θ_j represent the bus angles of system bus i and j, respectively, and S is the set of the whole system buses.

For convenience, we rewrite equations (1)–(3) as a brief form of expression as follows:

$$\begin{aligned} &\min\ f(\mathbf{X}, \mathbf{u}), \\ &s.t. \quad \begin{cases} \mathbf{h}(\mathbf{X}, \mathbf{u}) = \left[\mathbf{h}, \overline{\mathbf{h}}\right], \\ \mathbf{g}^{\min} \le \mathbf{g}(\mathbf{X}, \mathbf{u}) \le \mathbf{g}^{\max}, \end{cases} \end{aligned} \tag{5}$$

where $\mathbf{X}$ is the state variables vector, which consists of voltage magnitude of load buses, bus angle of nonslack bus, and reactive power generation. $\mathbf{u}$ represents control variables vector, including the VAR compensation of capacitors, voltage magnitude of generators, ratios of transformers. $\mathbf{h}(\mathbf{X}, \mathbf{u}) = [\mathbf{h}, \overline{\mathbf{h}}]$ stands for the power balance equations, and $\mathbf{h}$ and $\overline{\mathbf{h}}$ are lower and upper bounds of input data. $\mathbf{g}^{\min} \le \mathbf{g}(\mathbf{X}, \mathbf{u}) \le \mathbf{g}^{\max}$ represents the inequation constraints. Obviously, equation (5) belongs to a mixed integer nonlinear programming model with interval variables, and the improved PSO is adopted to solve it.

Here, we first construct a penalty for addressing the inequation constraints of interval variables, because it is quite time-consuming if we deal with the constraints of state variables directly during the PSO optimization process. In detail, we define the following quadratic penalty function of the interval variable $= [X, \overline{X}]$, where X and $\overline{X}$ are the present minimum and maximum values of X, respectively.

$$p(X) = \begin{cases} 1000 * \left(x^{\min} - \underline{\mathbf{X}}\right)^2, & \text{if } \underline{\mathbf{X}} < x^{\min}, \\ 0, & \text{if } \underline{\mathbf{X}} > x^{\min} \text{ and } \overline{\mathbf{X}} < x^{\max}, \\ 1000 * \left(\overline{\mathbf{X}} - x^{\max}\right)^2, & \text{if } \overline{\mathbf{X}} > x^{\max}. \end{cases} \tag{6}$$

Here, $x^{\min}$ and $x^{\max}$ are the lower and upper limit constraints of $\mathbf{X}$, respectively.

Therefore, in the PSO process, we will replace the original objective function f by a new objective function F, which is expressed by the following equation:

$$\min F = f(\mathbf{X}, \mathbf{u}) + p(\mathbf{X}). \tag{7}$$

3. Solution Method for the MRPOIU

In this section we first introduce an IPF algorithm based on the OSM. Secondly, the data-driven method is used to correct the interval of uncertain variables, and then several strategies are used to improve PSO. Finally, we introduce the algorithm framework for solving the RPOIU.

3.1. OSM-Based IPF Algorithm. The OSM-based IPF algorithm applied herein is a kind of direct optimization class of the IPF algorithm, which can avoid the expansion of the interval solution, and thereby obtain an IPF solution directly. The OSM-based IPF algorithm considers all possible states. Therefore, the interval range of the solution is closer to the actual state than the solutions obtained via interval iteration arithmetic and interval affine arithmetic [17].

The OSM follows extreme value theory, which requires deterministic power flow solutions corresponding to interval solutions for any uncertain input variables. In other words, when the control variables of the power systems are determined, the power flow solution changes with the uncertainty of the input variables. Therefore, the upper and lower boundaries of the IPF solution will be obtained on a closed interval of the input variable uncertainties. The OSM-based IPF algorithm applied herein is formulated in polar coordinates, and the solution method is transformed into an extreme value problem as follows:

$$\begin{aligned} &\max x_i \\ &\text{s.t.} \begin{cases} \mathbf{h}(\mathbf{x}) = \boldsymbol{\xi}, \\ \underline{\mathbf{h}} \le \boldsymbol{\xi} \le \overline{\mathbf{h}}, \end{cases} \\ &\min x_i \\ &\text{s.t.} \begin{cases} \mathbf{h}(\mathbf{x}) = \boldsymbol{\xi}, \\ \underline{\mathbf{h}} \le \boldsymbol{\xi} \le \overline{\mathbf{h}}, \end{cases} \end{aligned} \tag{8}$$

where x_i is the state variable of the power grid, $\mathbf{h}(\mathbf{x}) = \xi$ is the power flow constraint equation, and $\overline{\mathbf{h}}$ and $\mathbf{h}$ are the respective upper and lower bounds of the input variable uncertainties. The extreme value problem in equation (8) is a continuous linear equation that can be solved using the interior point method (IPM), which is conducted as follows.

Step 1: First set the values of all parameters required by the IPM, and input these parameters to the IPM along with the required data.

Step 2: Construct a series of optimization models with the state variable x_i and line power flow P_{ij} of the IPF as the objective function through equation (10).

Step 3: Solve equation (10) using the IPM to obtain the corresponding value of each state variable x_i and line power flow P_{ij}, and then obtain the interval range of each x_i and P_{ij}. Finally, output the results.

3.2. A Data-Driven Method for Reducing Conservatism of Interval Uncertainties. The historical data applied herein is the active power outputs of wind farms in Belgium sampled over one year in 2021 at one-hour intervals, which resulted in a set of 8760 data points. A cumulative probability distribution curve is fitted to the above sample data, and then the Monte Carlo direct sampling (MCDS) method is used to obtain the active power output intervals of the wind farm within a particular confidence level. The specific process is illustrated by the flowchart shown in Figure 1.

3.3. Improved PSO Algorithm. The improvement strategies applied herein to the PSO algorithm included the use of tent-based adaptive chaotic mapping to ensure that the initial particle population is truly scattered uniformly throughout the solution space [28], and an adaptive inertia weight adjustment strategy to balance the global exploration and local exploitation abilities of the PSO algorithm rationally, thereby avoiding premature convergence of the algorithm [29]. The flowchart and pseudocode of the proposed improved PSO algorithm are shown in Figures 2 and 3, respectively.

3.3.1. Tent-Based Adaptive Chaotic Mapping. In this strategy, a chaotic variable x is mapped in the kth iteration ($k = 1, 2, \ldots, T_{\max}$) to the interval [0, 1]. The initial population of PSO is calculated as follows:

$$x^k = \begin{cases} 2x^{k-1}, & 0 < x^k \le 0.5, \\ 2\left(1 - x^{k-1}\right), & 0.5 < x^k \le 1, \end{cases} \tag{9}$$

$$x_j^1 = \frac{z_j^1 - z_{\min,j}}{z_{\max,j} - z_{\min,j}}, \tag{10}$$

$$z_j^k = z_{\min,j} + x_j^k\left(z_{\max,j} - z_{\min,j}\right), \tag{11}$$

where j is the dimension of the particle ($j = 1, 2, \ldots, N$), z is the original spatial variable, and $z_{\max,j}$ and $z_{\min,j}$ are the limiting values of z in the j th dimension of the kth iteration.

The specific steps of this strategy are as follows:

Step 1: An initial vector $z^1 = [z_1^1\, z_2^1 \ldots z_N^1]^{\mathrm{T}}$ is randomly generated in accordance with the constraints. Then, z^1 is mapped to the chaotic space through equation (10)

Step 2: Calculate the chaotic variable x^{k+1} based on equation (9) and obtain the new original space variable z^{k+1} based on equation (11)

Step 3: If $k < T_{\max}$, return to Step 2; otherwise, terminate the mapping process and output the initial population

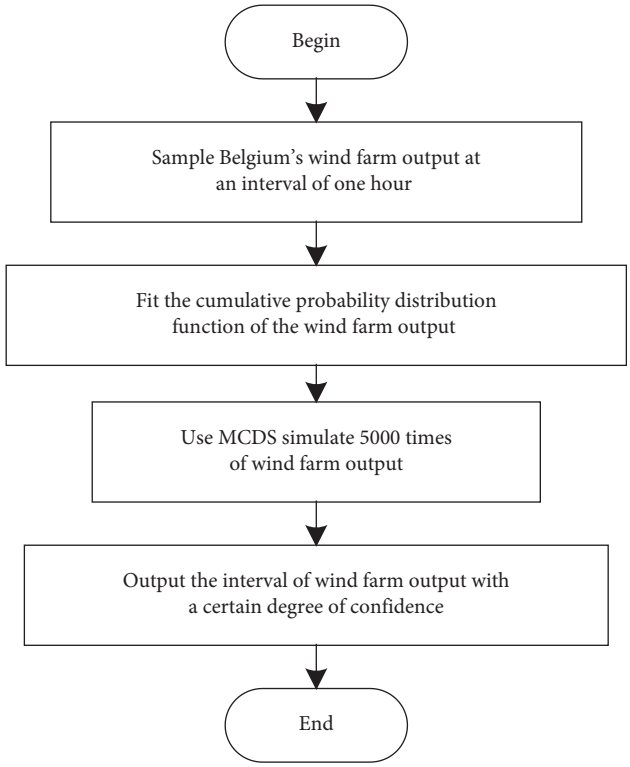

Figure 1: Historical data-driven process applied for modifying the intervals of uncertain input variables obtained by the IPF algorithm.

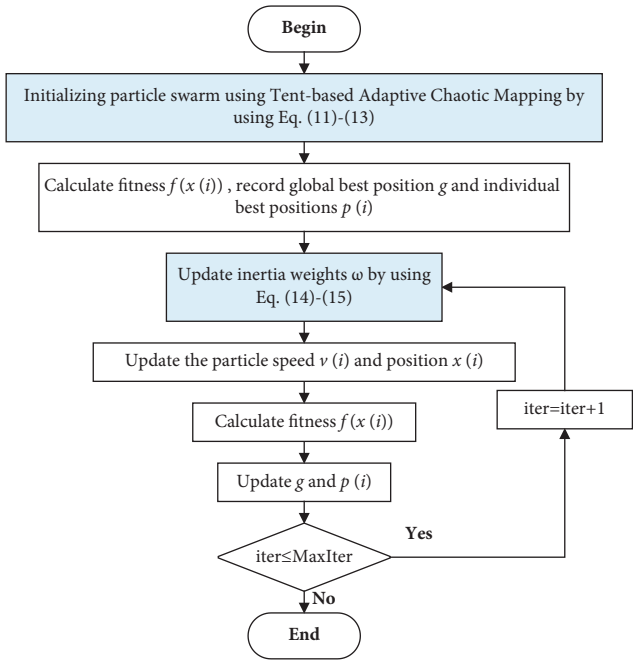

Figure 2: The flowchart of the improved PSO algorithm.

3.3.2. Adaptive Inertia Weight Adjustment. At the beginning of each iteration of PSO, G populations $(f_1, f_2, \ldots, f_G)$ are arranged in ascending order according to their fitness to form a new population sequence $(g_1, g_2, \ldots, g_G)$. The population with the greatest fitness, which is the population ranked first in the new population sequence (i.e., g_1), is denoted as the optimal particle, and the distance between the ith population g_i and g_1 is denoted as the optimal particle distance d_i. Then, the inertia weight ω of a particle is defined as follows:

$$\omega = u \cdot \left(\frac{\omega_s + (\omega_e - \omega_s) \cdot t}{T_{\max}} \right),$$

$$u_i = \begin{cases} 1 + \alpha, & d_i \geq S_2 G, \\ 1, & S_1 G \leq d_i \leq S_2 G, \\ 1 - \beta, & d_i \leq S_1 G, \end{cases} \tag{12}$$

where u_i is the control factor of the value of ω for the i th particle, where $u_i \in u$, ω_s, and ω_e are the respective initial and final values of ω, t is the current iteration number ($t = 1, 2, \ldots, T_{\max}$), α and β are adjustment parameters, where $\alpha > 0$ and $\beta > 0$, and S_1 and S_2 are the control parameters, where $S_1 < S_2 < 1$. These parameters play a critical role in determining the search behavior and convergence speed of the algorithm. Specifically, α and β control the global and local search speed of the algorithm, while S_1 and S_2 determine the proportion of particles that focus on local and global search, respectively. By choosing the appropriate values for these parameters, we can balance the trade-off between exploration and exploitation of the PSO, prevent premature convergence, and achieve better convergence rates.

3.4. Overall Framework of Solving the IRPOM by the Improved PSO. The overall framework of the solution process is illustrated by the flowchart shown in Figure 4. As shown in the flowchart, the uncertain input variable intervals are first obtained and then adjusted according to the proposed data-driven method. Then, the MRPOIU is solved using the improved PSO. At each iteration, the UPF is solved using the OSM-based IPF algorithm, which obtains the real power losses and determines whether each state quantity, such as voltage, power flow, and generator output, exceeds its limit. Finally, when the objective function (1) of MRPOIU converges to a certain precision, output results.

4. Simulation Results

The effectiveness and applicability of the proposed IRPOM are evaluated based on computational results obtained for a modified IEEE 30-bus system that includes wind power generators with rated power outputs of 10 MW or 20 MW according to two test cases. In case 1, we compare the RPO results obtained by the IRPOM with and without applying the data-driven interval modification approach, along with rated wind power generator outputs of 10 MW. The same conditions are applied in case 2, except that two extreme scenarios (scenario 1 and scenario 2) are added to verify the security and stability of the IRPOM. In scenario 1, the load and active generator output fluctuation ranges are assumed

Algorithm: The improved PSO

Input: MaxIter, Number of Population (N), Dimension (D)
Output: The global optimum
Begin
Initializing particle swarm: using Tent based Adaptive Chaotic Mapping by using Eq. (11)-(13).
Determine individual best position p (i) and global best position g.
While iter <= MaxIter
  For i=l to N
    Update inertia weights by using Eq. (14)-(15).
    Update particle speed v (i) and position x (i).
    Calculate fitness value $f(x(i))$.
    If $f(x(i)) < f(p(i))$, update the individual best position: $p(i) = x(i)$.
    If $f(x(i)) < f(g)$, update the global best position: $g = x(i)$.
  End for
End While
Return to the global best position g.
End

Figure 3: The pseudocode of the improved PSO algorithm.

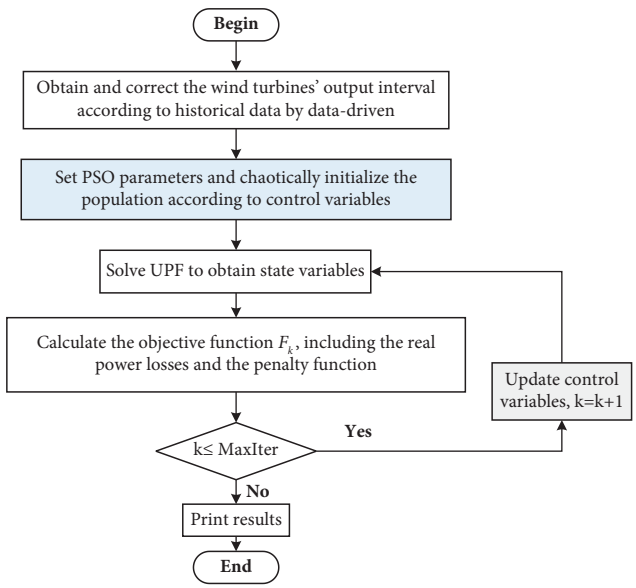

Figure 4: The overall framework of the applied improved PSO for solving the IRPOM.

to be 25%. In scenario 2, the load and generator active output fluctuation ranges are 20%, and the rated wind power generator outputs are 20 MW. Because the MCS method is generally regarded as an effective probabilistic method to solve uncertain problems, we applied this method 10,000 times to obtain realistic upper and lower limits for state variables in both cases 1 and 2, which then serve as basic references for comparison with the corresponding intervals obtained by the IRPOM. All numerical results are obtained using MATLAB 2019b operating on a computer with an Intel Core i5-8265U-1.6 GHz CPU with 16 GB of RAM.

4.1. Simulation Results under Modified IEEE 30-Bus System. As shown in Figure 5, the modified IEEE 30-bus system contains five conventional generators, three wind generators, four capacitors, and four transformers. As can be seen, buses 10, 16, and 24 are all connected to wind power generator units with constant power factors of $\cos\varphi = 0.95$. For ease of description, the order of bus numbers in the test system has been rearranged, with the slack bus first, followed by conventional generator buses and load buses. The component specifications applied herein, including the positions in the network, limits, and step sizes, are listed in Table 1. Unless otherwise specified, this article assumes that the fluctuation range of the load power and the active power of conventional generators is ±20%, that is, they are uniformly distributed within the range of $[0.8, 1.2] * a$, with a standard deviation of $\sqrt{3}a/15$, and a is the data of the standard IEEE 30-bus system. The correlation between variables is not considered. In addition, the service life of the reactive power compensation devices is assumed to be $T_\delta = 15$, the unit capacity investment cost ρ_c, ρ_l is 70 ¥/KVar (including postmaintenance management costs), and the grid electricity price is 0.5 ¥/KWh. All parameters are valued according to a per unit (p.u.) basis, and the basic power is set to 100 MVA.

4.1.1. Correction of Wind Farms Output through Data-Driven. The probability cumulative curve obtained by fitting the 8760 active power output data points is presented in Figure 6(a). Figure 6(b) shows the probability density curve of this set of data. As can be seen, the output of the wind farms never reaches a full load state. Subsequently, the active power output interval is modified with a 94% confidence level by applying the MCDS method, which reduces the active power output interval from its most conservative range of [0, 1] down to [0.006, 0.961]. Accordingly, the conservatism of the interval optimization calculation is reduced.

4.1.2. Optimization Results of the IRPOM. The control variables obtained through the IRPOM are presented in Table 2. No reactive power compensation devices are connected within the system before optimization, and the real power losses are 13.68 MW. After optimization, the system is

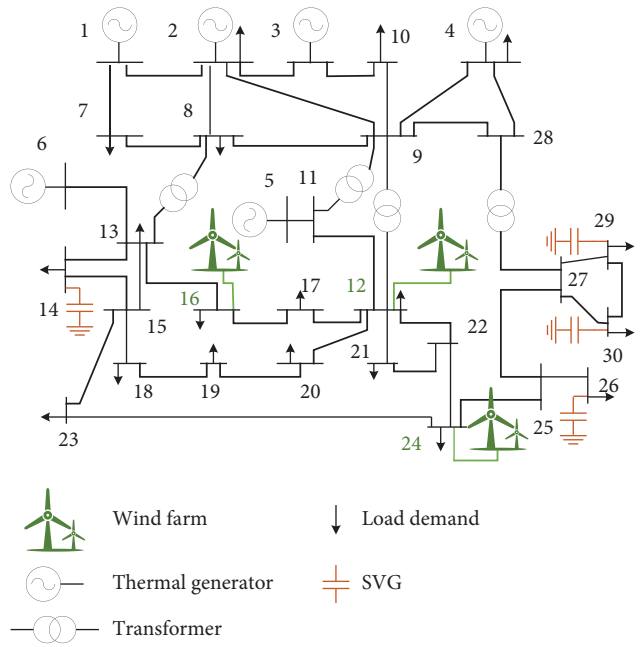

Figure 5: Network topology of the modified IEEE 30-bus system.

Table 1: Component specifications applied in the modified IEEE 30-bus system.

Control variable type	Position	Lower limit (p.u.)	Upper limit (p.u.)	Step size (p.u.)
Static VAR compensator outputs	Bus 14	0	0.25	0.01
	Bus 26	0	0.25	0.01
	Bus 29	0	0.25	0.01
	Bus 30	0	0.25	0.01
Ratios of transformers	Branch 6–9	0.9	1.1	0.05
	Branch 6–10	0.9	1.1	0.05
	Branch 4–12	0.9	1.1	0.05
	Branch 27-28	0.9	1.1	0.05
Voltages of generators	V_{G1}	0.9	1.1	—
	V_{G2}	0.9	1.1	—
	V_{G3}	0.9	1.1	—
	V_{G4}	0.9	1.1	—
	V_{G5}	0.9	1.1	—
	V_{G6}	0.9	1.1	—

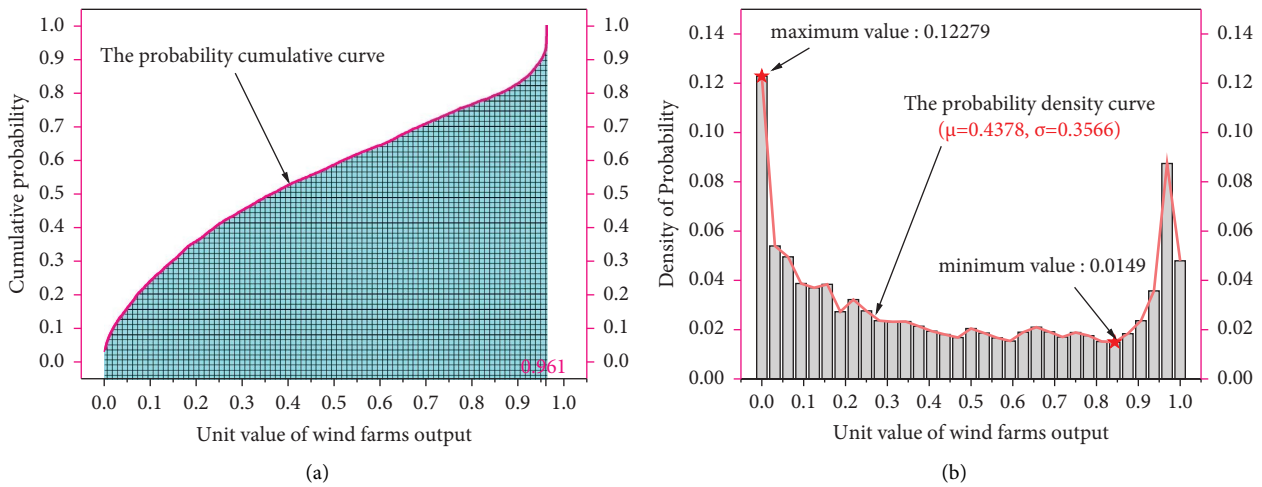

Figure 6: Probability cumulative curve (a) and probability density curve (b) obtained for the active power output of wind farms.

Table 2: Control variables used in solving the interval-based model.

Control variable type	Position	Results of IRPOM (p.u.)	Control variable type	Position	Results of IRPOM (p.u.)
Static VAR compensator outputs	Bus 14	0.24	Voltages of generators	V_{G1}	1.0719
	Bus 26	0.13		V_{G2}	1.0511
	Bus 29	0.14		V_{G3}	1.0140
	Bus 30	0.10		V_{G4}	1.0260
Ratios of transformers	Branches 6–9	0.90		V_{G5}	1.0567
	Branches 6–10	1.05		V_{G6}	1.0882
	Branches 4–12	1.00		—	—
	Branches 27–28	1.10		—	—

connected to 61 sets of compensation devices, and the real power losses are 6.28 MW. Therefore, the real power losses are reduced by 7.4 MW. According to function (1), the average annual cost of the energy losses before optimization is 59.9184 million yuan, and the average annual investment cost of reactive power compensation devices is 0 million yuan. After optimization, the annual average cost of the energy losses is 27.5064 million yuan, and the annual average investment cost of reactive power compensation devices is 0.2846 million yuan. This total cost of 27.7910 million yuan obtained after optimization represents a total cost that has been reduced by 32.7274 million yuan compared to the preoptimization cost. As can be seen, the proposed IRPOM significantly reduces the energy losses of the electricity grid and greatly improves its overall economy.

4.2. Comparison between Improved PSO, I-GWO, and GA. To evaluate the performance of the proposed improved PSO algorithm, we conducted a comparative validation with the genetic algorithm (GA) and the improved grey wolf optimizer (I-GWO) [30]. In this experiment, the parameters of the comparison algorithm are shown in Table 3. Figure 7 presents the midpoint of the objective function values for each iteration of the three algorithms. It is worth noting that the objective function value F considered here include the midpoint of the real power losses $f(X, \mu)$ and the penalty function values (X). Figure 7(a) shows that the improved PSO algorithm exhibits a more stable convergence behavior compared to the I-GWO algorithm. After around 70 iterations, the objective function value stabilizes and reaches a relatively low level with the improved PSO algorithm. However, the I-GWO algorithm shows slower convergence and fails to reach a satisfactory solution within the same number of iterations. Figure 7(b) shows that although the genetic algorithm can converge quickly, it also experiences premature convergence and gets trapped in local optima. These findings demonstrate the superior convergence and quality of the optimal solution achieved by the proposed improved PSO algorithm.

4.3. Case 1: Check the Conservatism of the IRPOM. The ranges of load voltage magnitudes and reactive power outputs obtained at each corresponding bus of the modified IEEE 30-bus system by the proposed IRPOM with and without applying the data-driven modification to the intervals are presented in Figures 8 and 9, respectively. The realistic upper and lower limits obtained by MCS for comparison are included here. Meanwhile, we present the differences between the upper and lower limits of the load voltage (i.e., the load voltage intervals) obtained at each system bus with and without applying the data-driven modification in Figure 10. The results in Figures 8 and 9 demonstrate that the voltage and reactive power output of each bus of the system never exceed their limits when applying the data-driven modification to the intervals. Hence, the proposed data-driven modification in the IRPOM ensures the safe operation of the power grid. Nonetheless, the results in Figure 8 demonstrate that the load voltage interval obtained for each bus by the data-driven methodology is nearly always narrower than that obtained without the modification. Accordingly, these results further demonstrate that the data-driven modification can reduce the conservativeness of the uncertain variable intervals.

4.4. Case 2: Check the Security of the IRPOM. The load voltage magnitudes and reactive power outputs obtained at each corresponding bus of the modified IEEE 30-bus system by the proposed IRPOM under scenario 1 are presented in Figure 11, along with the realistic upper and lower limits obtained by MCS for comparison. As can be seen, each reactive power output and load voltage lie within safe ranges, and none exceed the established limits.

The load voltage magnitudes and reactive power outputs obtained at each corresponding bus of the modified IEEE 30-bus system by the proposed IRPOM under scenario 2 are presented in Figure 12, along with the realistic upper and lower limits obtained by MCS. As can be seen, bus 11 has a voltage magnitude that exceeds the upper limit. This phenomenon can be assessed according to the simulated voltage magnitudes presented for bus 11 in Figure 13. According to these results, only 87 violations occurred in 10,000 Monte Carlo simulations, which represents a 99.13% confidence level. Therefore, the results obtained for scenario 2 are acceptable. Figure 14 demonstrates that the real power losses in both extreme scenarios can converge, thus further verifying that our algorithm can converge to satisfactory results in extreme cases.

The results of case 2 demonstrate that the IRPOM employing data-driven interval values can adapt to the uncertainty of wind power generators even under high renewable energy penetration and high fluctuation conditions.

Table 3: Parameters settings.

Algorithms	Settings
GA	Population size = 50, iterations = 200, crossover probability = 0.6, mutation probability = 0.01, and selection method: tournament selection
I-GWO	Population Size = 50, iterations = 200, and a was linearly decreased from 2 to 0
Improved PSO	Population Size = 50, iterations = 200, inertia weight = [0.4, 0.9], $\alpha = 0.5$, $\beta = 0.3$, $S_1 = 0.2$, $S_2 = 0.8$, and $c1 = c2 = 2$

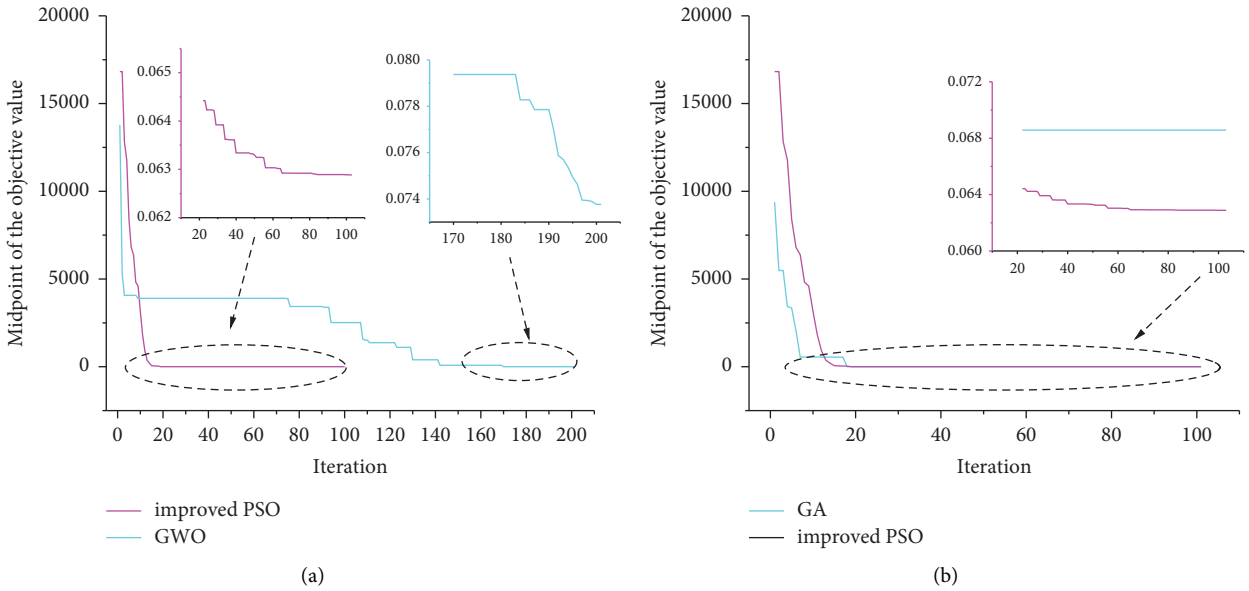

Figure 7: Midpoint of the objective function value of the IEEE30 system in each iteration of the algorithm. (a) Comparison between improved PSO and I_GWO. (b) Comparison between improved PSO and GA.

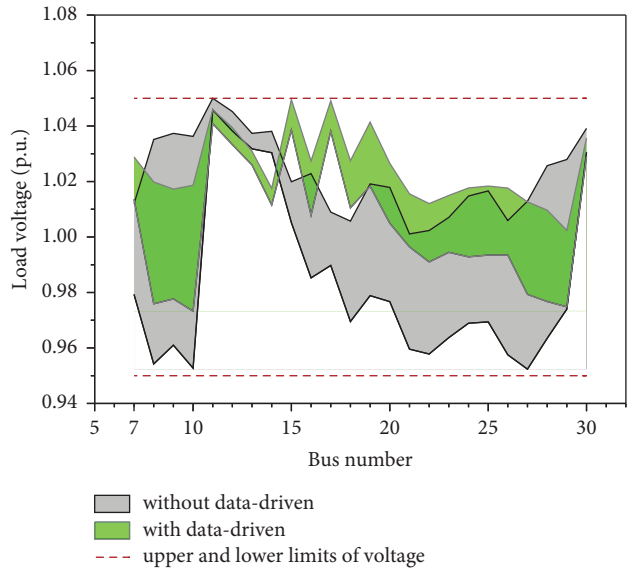

Figure 8: Load voltage magnitudes obtained at each bus of the modified IEEE 30-bus system.

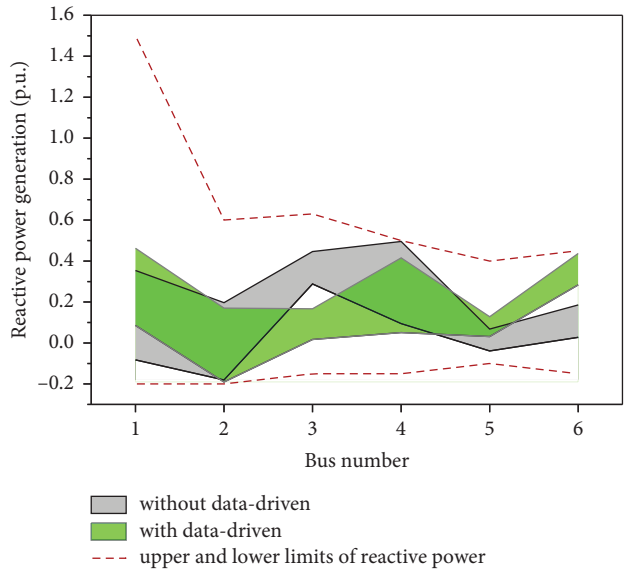

Figure 9: Reactive power outputs obtained at each bus of the modified IEEE 30-bus system.

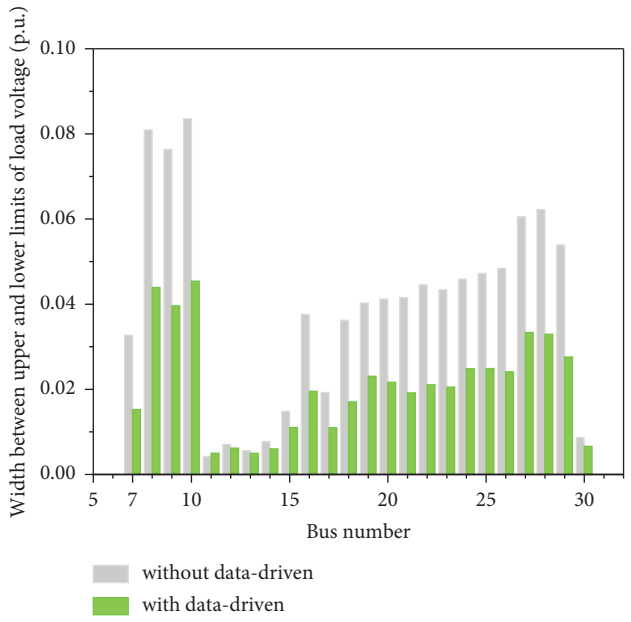

Figure 10: Interval width of load voltage magnitudes obtained by the IRPOM.

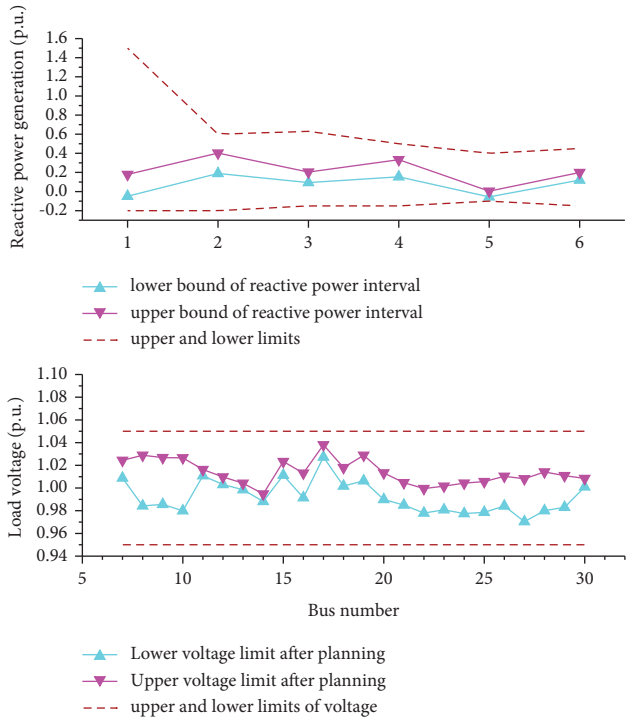

Figure 11: Load voltage magnitudes and reactive power outputs obtained at each bus under scenario 1.

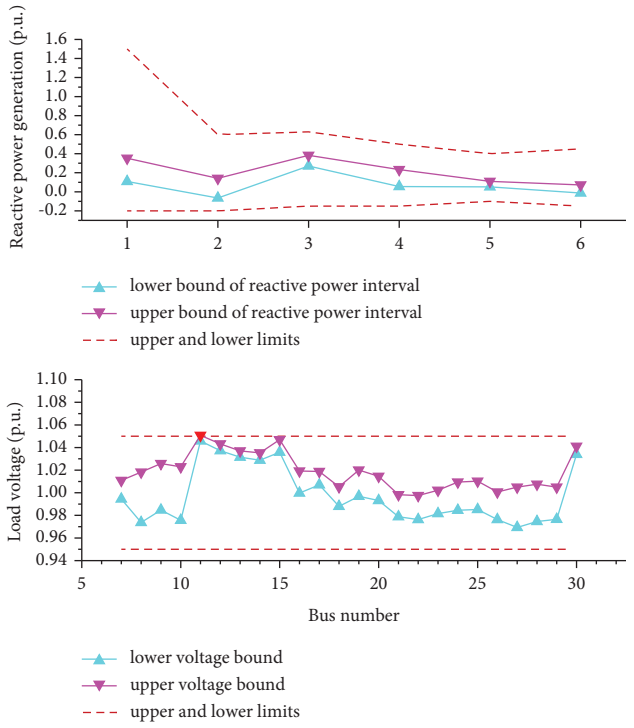

Figure 12: Load voltage magnitudes and reactive power outputs obtained at each bus under scenario 2.

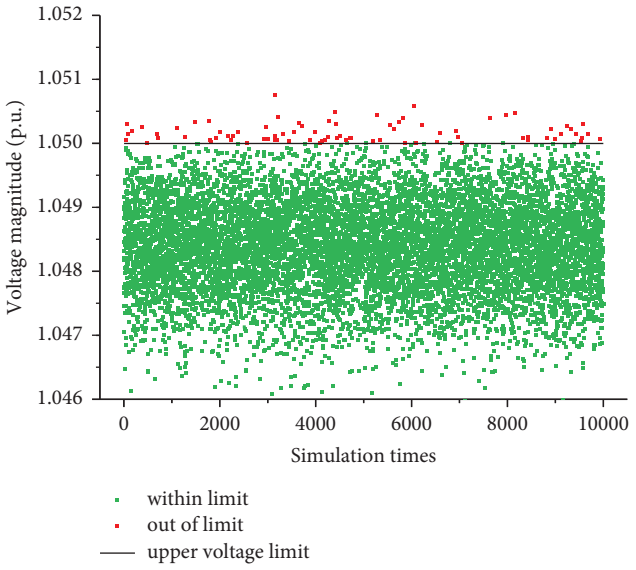

Figure 13: Results of Monte Carlo simulations for the voltage magnitude obtained at bus 11 under scenario 2.

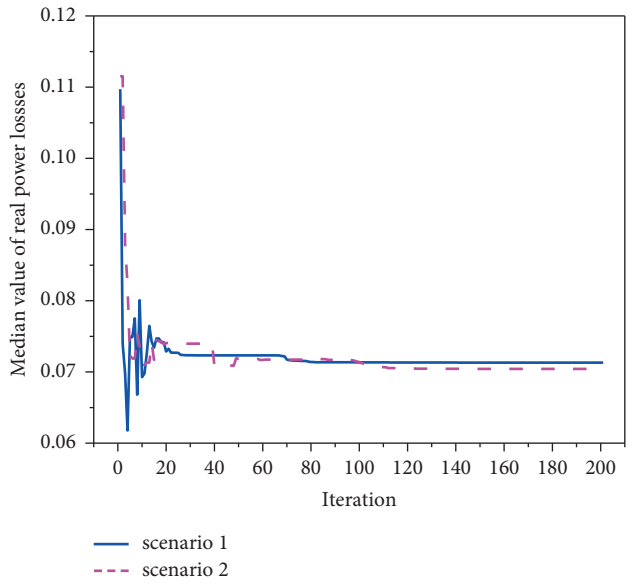

Figure 14: Midpoint of the real power losses in each iteration under scenarios 1 and 2.

Therefore, the obtained optimization solutions can ensure the safe and stable operation of electric power systems and reduce the accident rate and real power losses.

5. Conclusion and Future Research

The present work proposed a data-driven-based IRPOM to address the voltage security problem caused by uncertainties associated with wind power generator outputs. The IRPOM seeks to find a reactive power compensation scheme with the lowest power losses and the lowest cost while ensuring that state variables remain within their operating limit constraints. The IRPOM is solved with an improved PSO as the main framework. At each iteration, an OSM-based IPF algorithm is applied to calculate the uncertain power flow intervals, and a data-driven methodology is applied to reduce the conservatism of the optimized intervals. The performance of the proposed IRPOM is validated by numerical computations involving a modified IEEE 30-bus system. An analysis of the obtained results demonstrated that the proposed data-driven modification in the IRPOM ensures the safe operation of the power grid, while clearly reducing the conservativeness of the uncertain variable intervals. Moreover, the IRPOM can adapt to the uncertainty of wind power generators even under high renewable energy penetration and high fluctuation conditions, such that the obtained optimization solutions can ensure the safe and stable operation of electric power systems and reduce the accident rate and real power losses.

Similar to existing interval algorithms, the proposed algorithm in this paper only requires the upper and lower bounds of uncertain quantities, making the modeling relatively straightforward. However, it disregards the probabilistic information of the uncertain quantities and does not consider the interval correlation among different input uncertainties. Therefore, simultaneously exploring the available probability information while preserving the advantages and characteristics of interval power flow analysis will become a research focus in future uncertainty power flow analysis to address the situations where the input uncertainties have sufficient or insufficient statistical information. Additionally, accurately calculating interval algorithms that account for interval correlation is a pressing issue that needs to be thoroughly investigated and addressed.

Nomenclature

$E(P_{\text{Loss}})$:	Annual energy losses
P_{Loss}:	Real power losses
C_δ:	Total reactive power compensation capacity
T_δ:	Service life of reactive power compensation devices
ρ_1:	Power grid price in ¥/KWh
ρ_2:	The unit capacity investment cost in ¥/KVar
P_i:	The nodal active power
Q_i:	The nodal reactive power
Q_{Ci}:	Reactive compensation at bus i
P_{Li}:	Active load demand at bus i
Q_{Li}:	Reactive load demand at bus i
$P_{Li}, \overline{P_{Li}}$:	Lower and upper bounds of active load demand at bus i
$Q_{Li}, \overline{Q_{Li}}$:	Lower and upper bounds of reactive load demand at bus i
$P_{Gi}, \overline{P_{Gi}}$:	Lower and upper bounds of active power generation at generator bus i
Q_{Gi}:	Reactive power generation of generator bus i
Q_{li}, Q_{ci}:	Compensation capacity of the reactor and capacitor at bus i
T_l:	Tap positions of transformers at branch l

V_i, V_j: Voltage magnitudes of system bus i and j
$Q_{Gi,\min}, Q_{Gi,\max}$: Lower and upper bounds of the reactive power generation of generator bus i
$Q_{li,\min}, Q_{li,\max}$: Lower and upper bounds of the compensation capacity of the reactor at bus i
$Q_{ci,\min}, Q_{ci,\max}$: Lower and upper bounds of the compensation capacity of the capacitor at bus i
$T_{l,\min}, T_{l,\max}$: Lower and upper bounds of the tap positions of transformers at branch l
$V_{i,\min}, V_{i,\max}$: Lower and upper bounds of the voltage magnitudes of system bus i
n: Number of buses in power grid
θ_{ij}: $\theta_i - \theta_j$, where θ_i and θ_j represent the bus angles of system bus i and j
X: The state variables vector
u: The control variables vector.

Data Availability

No datasets are generated or analyzed during the current study.

Conflicts of Interest

The authors declare that they have no conflicts of interest regarding the publication of this article.

Acknowledgments

This work was supported by the Science and Technology Project of Changsha Power Supply Branch, State Grid Hunan Electric Power Company Limited (Grant no. 00FCJS2210147), the National Natural Science Foundation of China (Grant no. 52007056), and the Natural Science Foundation of Hunan Province, China (Grant no. 2020JJ5077).

References

[1] X. M. Liu, Y. Yue, X. Huang, W. Xu, and X. Lu, "A review of wind energy output simulation for new power system planning," *Frontiers in Energy Research*, vol. 10, 2022.
[2] N. Gupta, "A review on the inclusion of wind generation in power system studies," *Renewable and Sustainable Energy Reviews*, vol. 59, pp. 530–543, 2016.
[3] J. Y. Li, D. S. Xu, J. H. Wang, B. Zhou, M. H. Wang, and L. P. Zhu, "P2P multigrade energy trading for heterogeneous distributed energy resources and flexible demand," *IEEE Transactions on Smart Grid*, vol. 14, no. 2, pp. 1577–1589, 2023.
[4] S. D. Ahmed, F. Al-Ismail, M. Shafiullah, F. A. Al-Sulaiman, and I. M. El-Amin, "Grid integration challenges of wind energy: a review," *IEEE Access*, vol. 8, pp. 10857–10878, 2020.
[5] X. Q. Fu, "Statistical machine learning model for capacitor planning considering uncertainties in photovoltaic power," *Protection and Control of Modern Power Systems*, vol. 7, no. 1, p. 5, 2022.
[6] A. Ehsan and Q. Yang, "State-of-the-art techniques for modelling of uncertainties in active distribution network planning: a review," *Applied Energy*, vol. 239, pp. 1509–1523, 2019.
[7] A. M. Shaheen, S. R. Spea, S. M. Farrag, and M. A. Abido, "A review of meta-heuristic algorithms for reactive power planning problem," *Ain Shams Engineering Journal*, vol. 9, no. 2, pp. 215–231, 2018.
[8] F. Gami, Z. A. Alrowaili, M. Ezzeldien et al., "Stochastic optimal reactive power dispatch at varying time of load demand and renewable energsy resources using an efficient modified jellyfish optimizer," *Neural Computing and Applications*, vol. 34, no. 22, pp. 20395–20410, 2022.
[9] M. Aien, M. Rashidinejad, and M. F. Firuz-Abad, "Probabilistic optimal power flow in correlated hybrid wind-PV power systems: a review and a new approach," *Renewable and Sustainable Energy Reviews*, vol. 41, pp. 1437–1446, 2015.
[10] K. Honghai, S. Fuqing, C. Yurui, W. Kai, and H. Zhiyi, "Reactive power optimization for distribution network system with wind power based on improved multi-objective particle swarm optimization algorithm," *Electric Power Systems Research*, vol. 213, Article ID 108731, 2022.
[11] P. P. Biswas, P. N. Suganthan, R. Mallipeddi, and G. Amaratunga, "Optimal reactive power dispatch with uncertainties in load demand and renewable energy sources adopting scenario-based approach," *Applied Soft Computing*, vol. 75, pp. 616–632, 2019.
[12] Z. S. Li, J. H. Wang, H. B. Sun, F. Qiu, and Q. L. Guo, "Robust estimation of reactive power for an active distribution system," *IEEE Transactions on Power Systems*, vol. 34, no. 5, pp. 3395–3407, 2019.
[13] J. Liu, Y. F. Chen, C. Duan, J. Lin, and J. Lyu, "Distributionally robust optimal reactive power dispatch with wasserstein distance in active distribution network," *Journal of Modern Power Systems and Clean Energy*, vol. 8, no. 3, pp. 426–436, 2020.
[14] G. E. Constante-Flores and M. S. Illindala, "Data-driven probabilistic power flow analysis for a distribution system with renewable energy sources using Monte Carlo simulation," *IEEE Transactions on Industry Applications*, vol. 55, no. 1, pp. 174–181, 2019.
[15] M. Dadkhah and B. Venkatesh, "Cumulant based stochastic reactive power planning method for distribution systems with wind generators," *IEEE Transactions on Power Systems*, vol. 27, no. 4, pp. 2351–2359, 2012.
[16] N. Gupta, "Probabilistic optimal reactive power planning with onshore and offshore wind generation, EV, and PV uncertainties," *IEEE Transactions on Industry Applications*, vol. 56, no. 4, pp. 1–4213, 2020.
[17] C. Zhang, *Models and Algorithms of Reactive Power Optimization Considering Uncertainties Based on Interval Theory*, South China University of Technology Guangzhou, Guangzhou, China, 2018.
[18] B. R. Prusty and D. Jena, "A critical review on probabilistic load flow studies in uncertainty constrained power systems with photovoltaic generation and a new approach," *Renewable and Sustainable Energy Reviews*, vol. 69, pp. 1286–1302, 2017.
[19] A. R. Jordehi, "How to deal with uncertainties in electric power systems? A review," *Renewable and Sustainable Energy Reviews*, vol. 96, pp. 145–155, 2018.
[20] J. C. Lopez, J. Contreras, J. I. Munoz, and J. Mantovani, "A multi-stage stochastic non-linear model for reactive power planning under contingencies," *IEEE Transactions on Power Systems*, vol. 28, no. 2, pp. 1503–1514, 2013.
[21] A. Attarha, N. Amjady, and A. J. Conejo, "Adaptive robust AC optimal power flow considering load and wind power

uncertainties," *International Journal of Electrical Power and Energy Systems*, vol. 96, pp. 132–142, 2018.

[22] Y. Zhou, Z. S. Li, and G. R. Wang, "Study on leveraging wind farms' robust reactive power range for uncertain power system reactive power optimization," *Applied Energy*, vol. 298, Article ID 117130, 2021.

[23] M. Aien, A. Hajebrahimi, and M. Fotuhi-Firuzabad, "A comprehensive review on uncertainty modeling techniques in power system studies," *Renewable and Sustainable Energy Reviews*, vol. 57, pp. 1077–1089, 2016.

[24] C. Zhang, H. Y. Chen, Z. P. Liang, M. L. Guo, D. Hua, and H. Ngan, "Reactive power optimization under interval uncertainty by the linear approximation method and its modified method," *IEEE Transactions on Smart Grid*, vol. 9, no. 5, pp. 4587–4600, 2018.

[25] C. Zhang, Q. Liu, B. Zhou et al., "A central limit theorem-based method for DC and AC power flow analysis under interval uncertainty of renewable power generation," *IEEE Transactions on Sustainable Energy*, vol. 14, no. 1, pp. 563–575, 2023.

[26] X. Liao, K. Liu, J. Le, S. Zhu, B. Li, and Q. Wu, "Review on interval power flow calculation methods in power system," *Proceedings of the CSEE*, vol. 39, no. 02, pp. 447–458+642, 2019.

[27] C. Zhang, H. Chen, K. Shi, M. Qiu, D. Hua, and H. Ngan, "An interval power flow analysis through optimizing-scenarios method," *IEEE Transactions on Smart Grid*, vol. 9, no. 5, pp. 5217–5226, 2018.

[28] H. Hui and J. Zhong, "Application study of tent mapping-based chaos adaptive PSO algorithm in excitation control system of synchronous generator," *Power System Technology*, vol. 35, no. 06, pp. 45–49, 2011.

[29] W. Z. Guo and G. L. Chen, "A new strategy of inertia weight adjust ment for particle swarm optimization," *Computer Engineering and Science*, vol. 29, no. 01, pp. 70–72+75, 2007.

[30] M. H. Nadimi-Shahraki, S. Taghian, and S. Mirjalili, "An improved grey wolf optimizer for solving engineering problems," *Expert Systems with Applications*, vol. 166, Article ID 113917, 2021.